Detection of the trend and seasonal variation in tropospheric NO_2 over China

R. J. van der A,[1] D. H. M. U. Peters,[1,2] H. Eskes,[1] K. F. Boersma,[1] M. Van Roozendael,[3] I. De Smedt,[3] and H. M. Kelder[1,2]

Received 17 August 2005; revised 9 December 2005; accepted 22 March 2006; published 30 June 2006.

[1] The results of a trend study on the tropospheric NO_2 column over China are presented, on the basis of measurements from the satellite instruments GOME and SCIAMACHY. From these observations, monthly averaged tropospheric NO_2 distributions are determined for the period 1996 to 2005 on a 1° by 1° grid. A linear model with a seasonal component is used to fit these time series. The variance and the autocorrelation of the noise are used to calculate the significance of the trend. The results show a large growth of tropospheric NO_2 over eastern China, especially above the industrial areas with a fast economical growth. For instance, Shanghai had a linear significant increase in NO_2 columns of 20% ± 6% per year (reference year 1996) in the period 1996–2005. The seasonal pattern of the NO_2 concentration shows a difference between east and west China. In the east a NO_2 maximum is found during wintertime, because of chemistry and anthropogenic activity. Contrary to this, in the western part of China the NO_2 concentration reaches a maximum in summertime. This spatial difference correlates with the population distribution of China. Since there is negligible anthropogenic activity in west China this difference in seasonality of NO_2 is attributed to natural emissions in west China.

Citation: van der A, R. J., D. H. M. U. Peters, H. Eskes, K. F. Boersma, M. Van Roozendael, I. De Smedt, and H. M. Kelder (2006), Detection of the trend and seasonal variation in tropospheric NO_2 over China, *J. Geophys. Res.*, *111*, D12317, doi:10.1029/2005JD006594.

1. Introduction

[2] Nitrogen oxides (NO_x = NO + NO_2) play an important role in atmospheric chemistry. NO_x has significant natural sources (e.g., lighting and soil emissions) and anthropogenic (e.g., biomass burning, fossil fuel combustion) sources. Global tropospheric NO_2 distributions are measured by the satellite instruments GOME (from 1995 to 2003) aboard ERS-2, SCIAMACHY (from 2002) aboard Envisat platform and OMI aboard EOS-AURA (from 2004) [*Leue et al.*, 2001; *Richter and Burrows*, 2002; *Martin et al.*, 2002; *Boersma et al.*, 2004]. The GOME instrument measures NO_2 columns with a resolution of 320 km by 40 km and has a global coverage of three days. The ground pixel measured by SCIAMACHY has the resolution of 60 km by 30 km. Global coverage is achieved after six days.

[3] Recent studies on the tropospheric NO_2 columns show that the satellite measurements are suitable for improving emission inventories and air quality studies. *Jaeglé et al.* [2004] used GOME measurements over the Sahel to map the spatial and seasonal variations of NO_x, mainly caused by biomass burning and soil emissions. *Martin et al.* [2003] used GOME measurements to derive a top-down emission inventory. The top-down inventory in combination with bottom-up emission inventory is used to achieve an optimized posterior estimate of the global NO_x emissions. *Boersma et al.* [2005] used GOME measurements to estimate the global NO_x production from lightning by comparing modeled and measured spatial and temporal patterns of NO_2 in the tropics. In the work by N. Blond et al. (Intercomparison of SCIAMACHY nitrogen dioxide observations, in situ measurements, and air quality modeling results over Western Europe, submitted to *Journal of Geophysical Research*, 2005), SCIAMACHY measurements are compared with an air quality model and ground measurements. They showed that SCIAMACHY measurements are able to monitor the air pollution over Europe and its day-to-day changes.

[4] In this study we focus on China for the period 1996 to 2005. China has one of today's fastest growing economies of the world. This increase in economic activity is accompanied by a strong increase of emissions of tropospheric pollutants and therefore leads to extra pressure on the environment. We will combine GOME and SCIAMACHY measurements to obtain a 9-year data set that is suitable for a trend study. The strong increase in NO_x emissions in China is due to a increase in industry and traffic, see *Wang and McElroy* [2004]. These emissions are concentrated on

[1] Royal Netherlands Meteorological Institute, De Bilt, Netherlands.
[2] Also at Department of Applied Physics, Eindhoven University of Technology, Eindhoven, Netherlands.
[3] Belgian Institute for Space Aeronomy, Brussels, Belgium.

0148-0227/06/2005JD006594

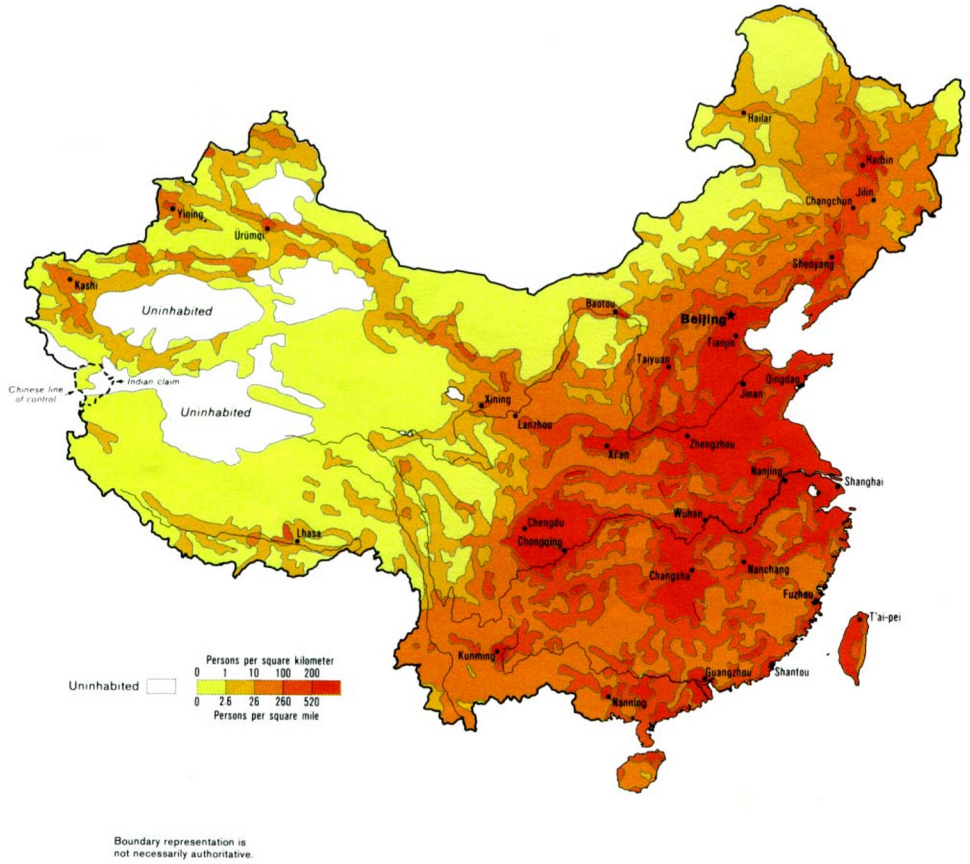

Figure 1. Population density in China. The red areas in east China are the major industrial and urbanized regions of China. (Courtesy of the University of Texas Libraries, the University of Texas at Austin.)

the densely populated and industrialized eastern part of China, as can be seen in Figure 1.

[5] The combination of the variability in meteorological conditions, chemistry and emissions leads to a seasonally dependent NO_2 concentration with an expected maximum of NO_2 in wintertime in regions with strong anthropogenic emissions. The NO_2 lifetime is on the order of one day depending on many factors like meteorological conditions, photolysis timescale and OH concentrations. A higher actinic flux results in a higher OH concentration (if the water vapor concentration is high enough), which reacts with NO_2 to form HNO_3, the principal sink for NO_x [e.g., *Jacob.*, 1999]. The emissions also show a variability. In wintertime, the anthropogenic emissions are expected to be higher because of heating of buildings, as shown for China by *Streets et al.* [2003]. *Beirle et al.* [2003] found a variability with a weekly pattern in the NO_2 concentration above Europe, related to reduced anthropogenic emissions during the weekend. Above China no significant weekly cycle was observed by *Beirle et al.* [2003].

[6] The first objective of this study is to quantify the trend in tropospheric NO_2 using satellite data over China. Our second objective is to use the data set to investigate the seasonality of the NO_2 columns over China. In section 2 a short introduction is given on tropospheric NO_2 retrieval method. The data analysis is described in section 3, which gives an overview of the applied model and statistics. The results of this study, the trend and the seasonal cycle of tropospheric NO_2 over China, are shown in sections 4 and 5. Finally in section 6 the conclusion and outlook of this study are presented.

2. Tropospheric NO_2 Retrieval

[7] The GOME and SCIAMACHY spectrometers measure backscattered light from the Earth in the UV and visible wavelength range. From the observed spectral features around 425–450 nm slant column densities (SCD) of NO_2 are derived with the Differential Optical Absorption Spectroscopy (DOAS) method [*Platt*, 1994]. The work presented here is based on slant columns retrieved from the satellite data by BIRA-IASB [*Vandaele et al.*, 2005]. The NO_2 stratospheric column is deduced from a chemistry-transport model assimilation run of the NO_2 slant column data. Subsequently, the assimilated stratospheric slant column is subtracted from the retrieved DOAS total slant column, resulting in a tropospheric slant column. The tropospheric NO_2 columns are derived from these slant columns, the conversion from slant to vertical column density is done with the air mass factor [*Boersma et al.*, 2004].

[8] The air mass factor (AMF) is the ratio between the measured slant column and the real vertical column. The AMF depends on the geometry of the measurement and the sensitivity of the instrument for the observed NO_2 concentrations. The sensitivity depends on surface albedo,

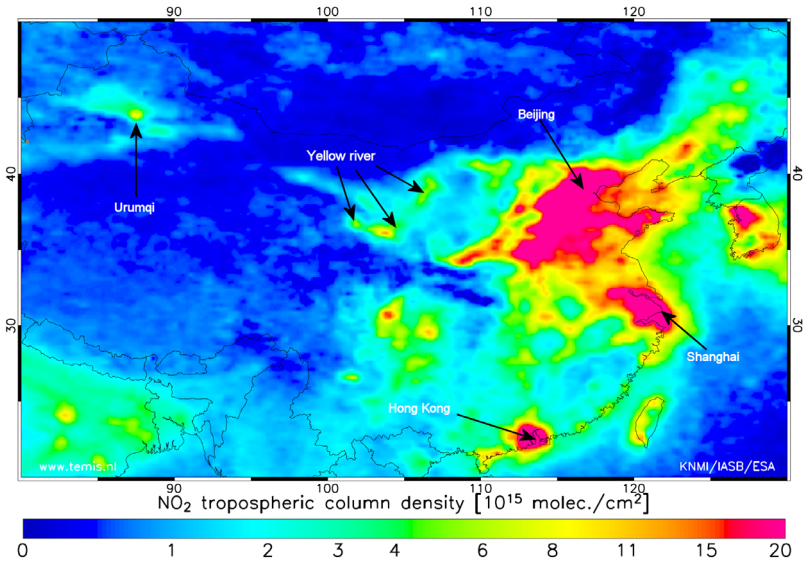

Figure 2. Yearly averaged tropospheric NO_2 column measured by SCIAMACHY for 2004.

vertical profile of NO_2, solar zenith angle, and cloud conditions. The a priori shape of the vertical profile is derived with the chemical-transport model TM4 [*Dentener et al.*, 2003]. It depends on meteorological fields from ECMWF and emissions from the EDGAR emission database extrapolated to the modeled year. Height-dependent AMF lookup tables are based on calculations with the Doubling-Adding KNMI (DAK) radiative transfer model. The tropospheric vertical column is retrieved using TM4 tropospheric model profiles (colocated for each GOME and SCIAMACHY pixel individually) and combined with albedo and cloud information. The latter consists of cloud fraction and cloud top height derived by the FRESCO algorithm [*Koelemeijer et al.*, 2003]. Only observations with an estimated cloud radiance of less than 0.5 are used in this study (cloud fraction less than about 0.2). The retrieval includes surface albedo values constructed from a combination of the TOMS-Herman-Celarier-1997 [*Herman and Celarier*, 1997] and Koelemeijer-2003 surface reflectivity maps (available on a monthly basis). No aerosol correction is applied. This choice is based on the realization that the cloud retrieval will be influenced by aerosol as well, and is further motivated by the error analysis presented in the work of *Boersma et al.* [2004]. The final NO_2 column data product is publicly available on the TEMIS project website (www.temis.nl) with detailed error estimates and kernel information [*Eskes and Boersma*, 2003]. In Figure 2 the year average tropospheric NO_2 column of 2004 is given. Figure 2 shows high concentration above the highly populated regions like Beijing, Shanghai, Hong Kong and South Korea. It can also be seen that the satellite is detecting the emissions around the Yellow River (Huang He). Over western China, low NO_2 columns are observed except over the large city Urumqi in the northwest.

3. Data Analysis

[9] The GOME data from March 1996 till March 2003 and the SCIAMACHY data from April 2003 till February 2005 have been used to analyze the trends and variability in NO_2 over China. April 2003 is the first month when SCIAMACHY NO_2 columns were retrieved successfully. The retrieved tropospheric NO_2 columns are gridded on a 1° by 1° grid, using weighting factors for the surface area overlap between satellite pixel and grid cell. The 1° by 1° grid is chosen to average out the effect of different satellite pixel sizes.

[10] For each cell two time series are determined; a time series based on a two weeks average and one based on a monthly average. Both time series are tested for the best fit with the model of equation (1), which will be explained below. Because twice as many satellite measurements are used for the monthly average as compared to the 2-weekly means, the monthly average leads to a better and more consistent time series with a lower autocorrelation. Therefore the analysis as presented in this study are based on monthly averages. The negligible weekly cycle of the NO_2 concentration above China makes it unnecessary to compensate for lower weekend measurements. The temporal variability in the NO_2 columns is usually larger than the precision of the measurements. To account for both effects, the uncertainty of the monthly mean is determined by taking the sample standard deviation of the mean. The measurement error on the tropospheric NO_2 for individual pixels as calculated by *Boersma et al.* [2004] shows a dependency on the absolute value of tropospheric NO_2, having a minimum error of about $1 \cdot 10^{15}$ molec/cm^2. This minimum error is used as lower limit for the error on the monthly average NO_2 concentration to avoid a nonrealistic accuracy caused by a limited number of samples.

[11] To fit the time series, a model with a linear trend and a seasonal component for the annual cycle of NO_2 has been used. This model is described by the following function based on *Weatherhead et al.* [1998],

$$Y_t = A + BX_t + C\sin(DX_t + E) + \delta U_t + N_t, \qquad (1)$$

where Y_t represents the monthly NO_2 column of month t and X_t is the number of months after January 1996, N_t is the remainder (residual unexplained by the fit function) and A,

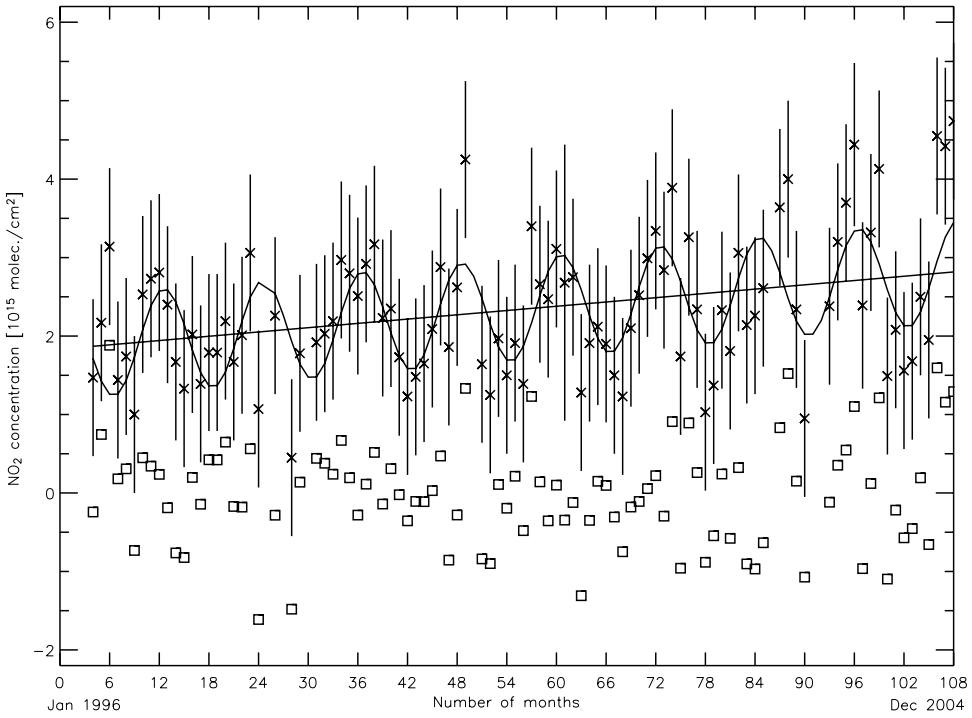

Figure 3. An example of a time series for one grid cell near Ji'an (115.5, 27.5). The *Y* axis shows the monthly mean NO_2 tropospheric column, and the *X* axis shows the month index starting January 1996. The crosses mark the measurements by GOME and SCIAMACHY. The solid line is the fitting result, consisting of a linear growth and a seasonal component. The difference between fit and measurement is marked by the open squares.

B, *C*, *D*, *E*, δ are the fit parameters. Parameter *A* represents the NO_2 column in January 1996, and *B* is the monthly trend in NO_2. The seasonal component contains amplitude *C*, a frequency *D* and a phase shift *E*. The fit of the frequency *D* leads to an expected period of one year, therefore this fit parameter was fixed to $\pi/6$ for the final analyses. The data have also been fitted with a linear model, without a seasonal component. The analyses of this fit showed that the seasonal component was an essential part of the model. A linear growth was used to fit the time series since fitting a linear growth instead of an exponential growth of the tropospheric NO_2 column over China resulted in slightly lower residuals for the period 1996 to 2005.

[12] To achieve more significant results both GOME and SCIAMACHY data are used. The term δU in equation (1) is used to fit the possible bias between the measurements, where δ is the value of the bias and U_t is,

$$U_t = \begin{cases} 0 & t < T_0 \\ 1 & t \geq T_0 \end{cases}. \tag{2}$$

In this equation the time T_0 ($0 < T_0 < T$) is the moment when the time series switches from using GOME to using SCIAMACHY data, which in this case is April 2003. The total number of months is denoted by *T*. The bias δ is fitted and checked for latitude dependence over China. We find that the bias is negligible, with values less than 0.01 10^{15} molec/cm^2. The performance of the GOME instrument was insufficient for our purpose after May 2003 and SCIAMACHY measurements are not available before 15 January 2003. The short remaining overlap period during 2003 is also used to check the consistency between both instruments. The average difference between measurements of GOME and SCIAMACHY in this period is (0.03 ± 0.16) 10^{15} molec/cm^2, which is very small considering the differences in the scenes (cloudiness, coverage) observed by the instruments. This consistency between the two instruments is also described by *Richter et al.* [2005]. On the basis of these results the bias term is set to zero in the analysis below.

[13] The remainder, N_t in equation (1) is the difference between the model and the measured value. *Weatherhead et al.* [1998] suggest modeling the remainder by

$$N_t = \phi N_{t-1} + \varepsilon_t, \tag{3}$$

where ε_t is the white noise and ϕ is the autocorrelation in the remainder. The autocorrelation in the remainder is a result from processes which are persistent with time and which are not described by the fit function, see *Tiao et al.* [1990]. We produced plots of the correlation between remainders as a function of the time difference. A typical autocorrelation of 0.1 is found, indicating that the remainders are only weakly correlated. The autocorrelation in the remainder affects the precision of the trend. In the work by *Weatherhead et al.* [1998] a derivation is given for the precision of the trend as function of the autocorrelation, the length *T* of the data set in months and the variance in the remainder, σ_N.

[14] The length of the data set in years, *n*, is introduced to express the precision of the trend per year. For small

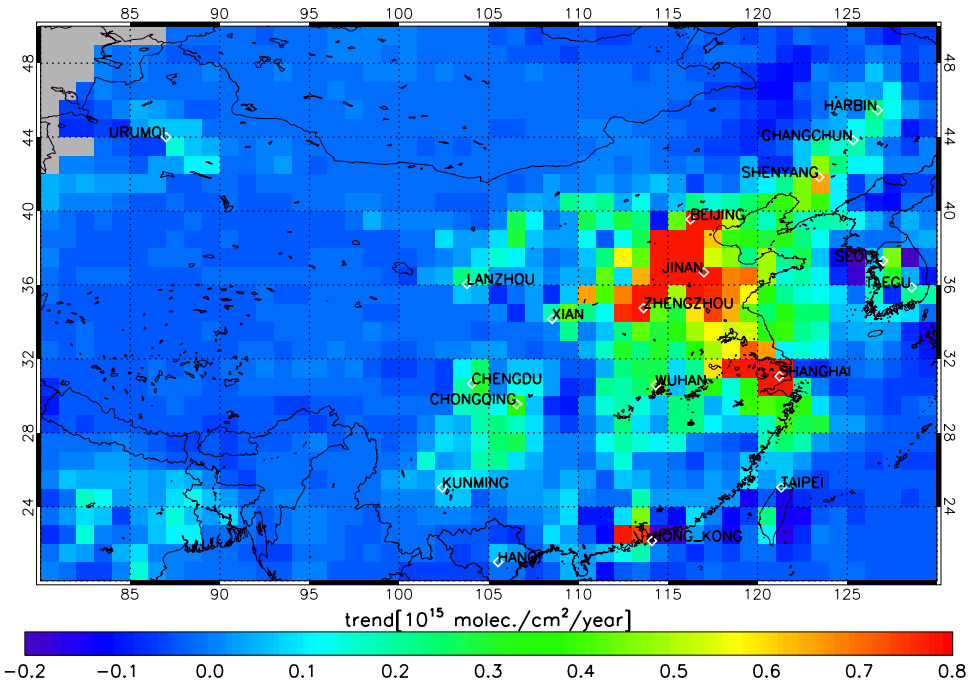

Figure 4. Trend of the NO_2 concentration over China for the period 1996–2004.

autocorrelations the standard deviation σ_B of the trend per year is approximately given by

$$\sigma_B \approx \left[\frac{\sigma_N}{n^{3/2}}\sqrt{\frac{1+\phi}{1-\phi}}\right]. \quad (4)$$

[15] Figure 3 shows an example of a measured time series and the fitted function. The monthly average tropospheric NO_2 vertical column density is plotted against the number of months after January 1996. The small crosses are the monthly averaged values measured by GOME and SCIAMACHY. The solid line is the model fit and the remainder between model and measurement is denoted by the squares.

4. Trend Analysis

[16] For each grid cell in China the model from equation (1), is applied, leading to a spatial distribution of each of the fitting parameters of the model. In Figure 4 the trend in NO_2 concentration is shown as the yearly increase in tropospheric NO_2. In Figure 4 it can be seen that the trend is the highest in the eastern part of China. These regions with the highest trend correspond to the regions with a fast industrial and economical development. The fastest growing economy is in the Shanghai region, which also shows the largest growth of tropospheric NO_2. It is interesting to note that the growth in the region around Hong Kong is less than for other regions with a high economical activity. This is probably due to the already high level of economic activity in 1996 when our trend study started and a package of measures against air pollution in Hong Kong over the last years.

[17] The precision σ_B of the trend on NO_2 is calculated using equation (4). It is a common decision rule for trend detection that a trend B is real with a 95% confidence level if $|B/\sigma_B| > 2$ [*Weatherhead et al.*, 1998]. In Figure 5 the trend is shown only for those grid cells that have a real trend. Figure 5 shows that a significant trend (colored grid cells) is detected in the regions of east China with a high population and high industrial activity. From equation (4) it can be seen that the standard deviation of the trend decreases if the length of the data set increases. Therefore it can be expected that for more grid cells a significant trend ($|B/\sigma_B| > 2$) can be detected with a longer data set. When only using GOME data in this analysis we get about the same results but with less significance. When adding SCIAMACHY data to this analysis the results became less noisy and more grid cells with significant results were obtained.

[18] In Table 1 the trend estimates and start values for some major cities are shown. A yearly growth is determined in terms of percentage with respect to the start value in 1996 to indicate the increase of the NO_2 column. It should be noted that that this percentage is given relative to the start value in 1996 because we applied a linear model. Shanghai is one of the fastest growing industrial areas, which is reflected in a large growth in NO_2. The growth rate in Shanghai is larger than in Beijing, since Shanghai is the economic centre of China including a harbor and industrial activities that are stimulated by the Chinese government. The trend over Taipei is not significant in this period. This is probably due to the effect of measures by the government to improve the air quality in Taiwan (these measures included subsidies on environmental-friendly techniques in traffic, improved public transport, and imposing pollution penalties).

[19] The increase of industrial and economical activity results in an increase of various types of emissions. For instance, an increase of aerosols may lead to higher sensitivity of the satellite measurements for NO_2 present within and above the aerosol layers. Therefore it is possible that a

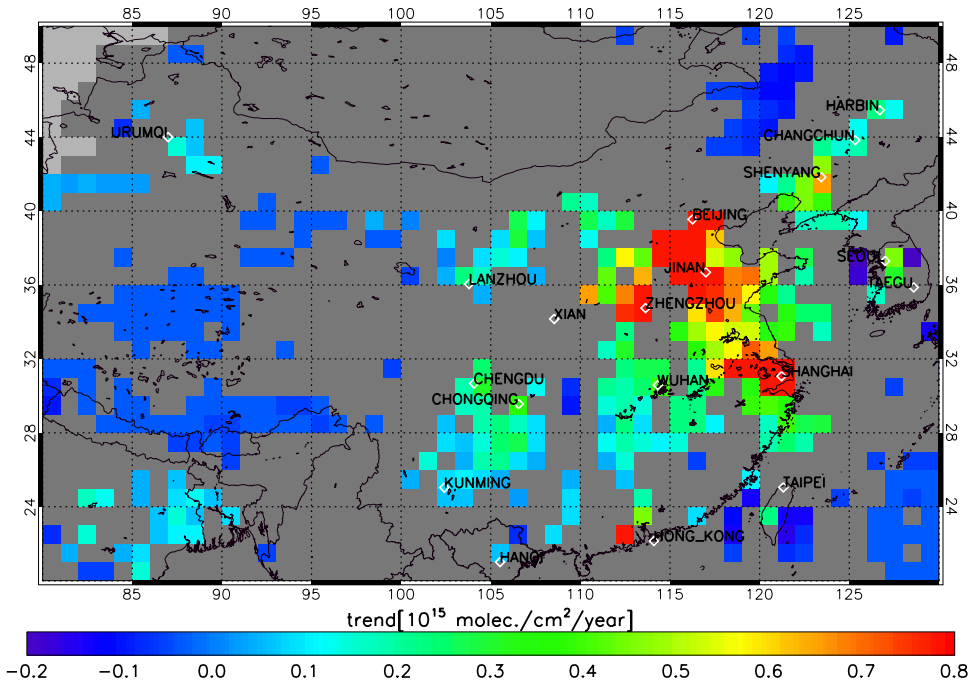

Figure 5. Same as Figure 4 but for the significant grid cells (grey areas are not significant). The significance is calculated as the NO_2 trend per year divided by the standard deviation. If this value is higher than 2 (colored areas) a real trend is indicated with a 95% confidence level.

measured trend in NO_2 concentration is enhanced by a trend in aerosols. However, *Boersma et al.* [2004] showed that satellite-derived cloud fractions are also sensitive to aerosols with a high single scattering albedo. An increase in cloud fractions as a result of higher aerosol concentrations leads to a similar AMF correction for aerosols as would be accomplished through a direct radiative transfer calculation without cloud correction. So, first of all, if there would be a distinct trend in scattering aerosols over China, its effect on NO_2 slant columns would be, to first order, compensated by increased cloud fractions. Secondly, a trend study of FRESCO monthly mean cloud fractions for situations with cloud fractions <0.2 showed no significant increase in cloud fraction nor an appreciable decrease in the number of available observations. This suggests that the effect of scattering aerosol changes in time on the derived trends in NO_2 may be neglected. The study by Boersma et al. also investigated the effects of 'absorbing' aerosol mixtures on trace gas and cloud retrievals. They found that the chances of finding appreciable increases (or decreases) in NO_2 slant columns or cloud fractions from strong increases in absorbing aerosols are small, as the single scattering albedo of absorbing mixtures is reported to be at least on the order of 0.8 [*Dubovik et al.*, 2002]. Hence, in the spirit of the above, we do not expect an appreciable effect of absorbing aerosols on our NO_2 trend results.

[20] The tropospheric slant column is calculated by subtracting the stratospheric slant column from the total slant column. To derive the vertical tropospheric column the tropospheric slant column is divided by the calculated

Table 1. Observed Trends for Some Cities in East Asia[a]

	Mean Concentration NO_2 in 1996, 10^{15} molec/cm^2	Linear Trend in NO_2, 10^{15} molec/cm^2/year	Error on Trend, 10^{15} molec/cm^2/year	Growth (Reference Year 1996)	Statistically Significant? (Y/N)
Beijing	11.6	1.2	0.50	(10 ± 4)%	Y
Seoul	10.3	0.36	0.22	(4 ± 2)%	Y
Pearl River Delta (Hong Kong)	8.0	0.68	0.49	(9 ± 6)%	N
Jinan	7.8	0.89	0.19	(11 ± 2)%	Y
Shanghai	6.7	1.3	0.34	(20 ± 5)%	Y
ShenYang	4.1	0.66	0.26	(16 ± 6)%	Y
Xian	3.8	0.21	0.12	(6 ± 3)%	N
Chengdu	3.7	0.32	0.07	(9 ± 2)%	Y
Taipei	3.7	−0.01	0.09	(0 ± 3)%	N
Chongqing	3.3	0.39	0.10	(12 ± 3)%	Y
Harbin	2.7	0.24	0.10	(9 ± 4)%	Y
Urumqi	1.4	0.15	0.04	(11 ± 3)%	Y
Background 86°E × 40°N	0.5	0	0.01	(0 ± 2)%	N

[a]Growth is the percentage calculated with respect to the year 1996.

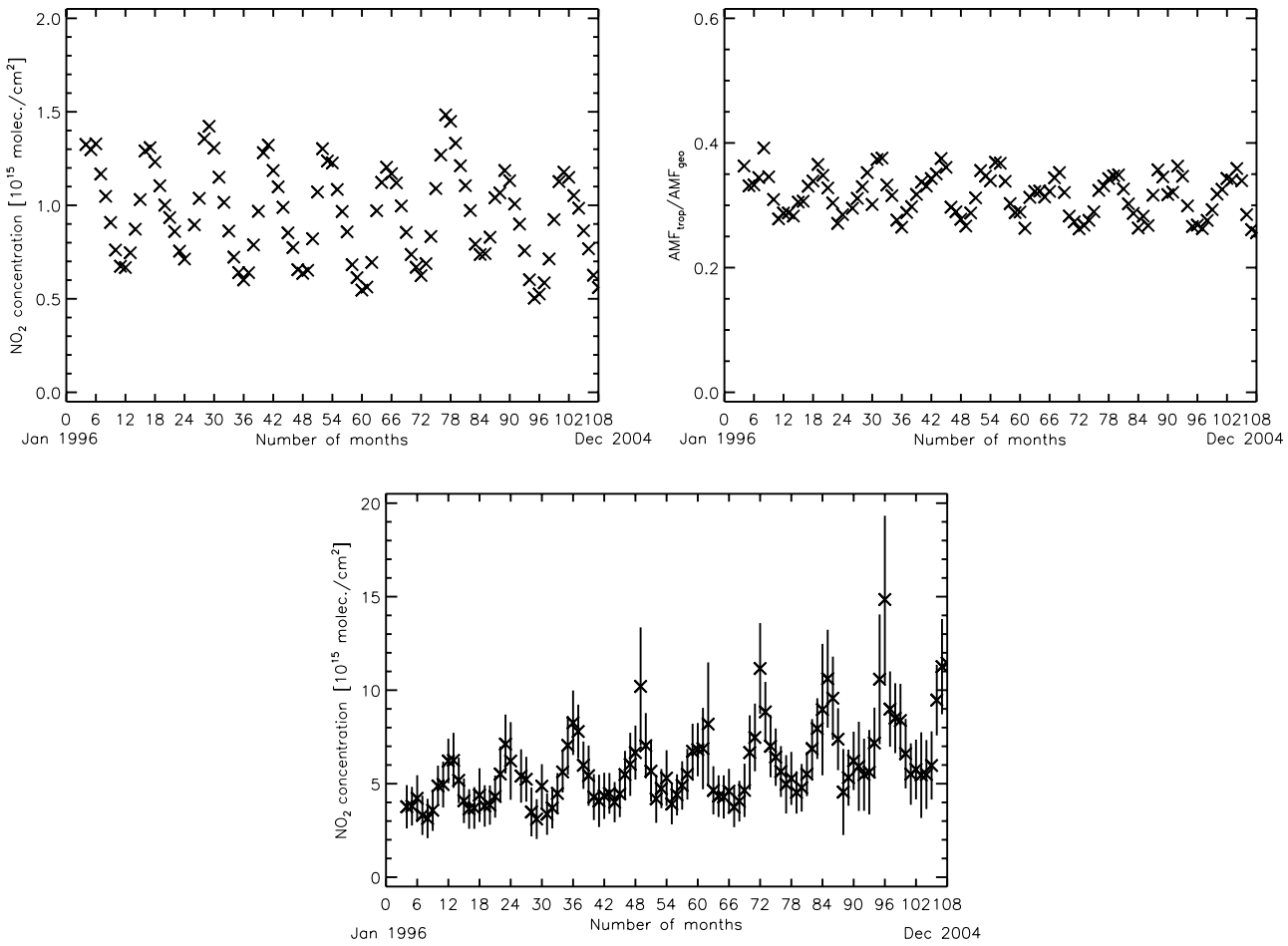

Figure 6. Time series of monthly averages of (bottom) the tropospheric vertical column, (top left) the stratospheric vertical column and (top right) the tropospheric air mass factor divided by the geometrical air mass factor. The monthly averages are calculated for east China (110–120°E, 20–40°N).

tropospheric air mass factor. An additional trend study is performed on the stratospheric column and the tropospheric air mass factor to make sure that the observed trend originates from the tropospheric column. In Figure 6 the time series are shown for the vertical stratospheric column, the tropospheric air mass factor and the tropospheric column. The time series are based on the monthly averages for east China (110–120°E, 20–40°N). The tropospheric air mass factor is divided by the geometrical air mass factor to compensate for the viewing geometry effects, see *Boersma et al.* [2004] for the definitions of the air mass factors. In Figure 6 it can be seen that there is a decreasing trend in the stratospheric column. This trend is between 0 and 2 percent per year, but it is never significant. This trend in stratospheric NO_2 can account for not more than 1 percent trend per year in the industrialized part of China. The tropospheric air mass factor shows a trend between −2 and +1 percent and it is often significant. The trend in NO_2 is inversely proportional to the trend in the AMF. This trend may be caused by changes in the NO_2 profile due to increased emissions or by changes in meteorological aspects like the temperature, boundary layer mixing, or cloud properties. To investigate the relation of the air mass factor trend and the observed trend in the tropospheric column, the spatial correlation is calculated between the relative yearly change in the air mass factor and the relative yearly change in the tropospheric column for all grid cells in east China. A small negative correlation of −0.14 is found for the geographical pattern of both trends. From this we conclude that there is not only a trend in tropospheric NO_2 but also changes in meteorological aspects. The small spatial correlation between the changes in the meteorological aspects and the trend in the NO_2 column led us conclude that the trend in the air mass factor is not contributing much to the trend in tropospheric NO_2.

5. NO_2 Seasonal Cycle

[21] Equation (1) is also used to study the seasonal cycle of the NO_2 concentration. The fitted phase shift, E, is used to determine in which month the seasonal maximum takes place. The seasonal maximum is found by taking the month number which is nearest to $3-6E/\pi$ (for positive C and E on the range $[-19\pi/12, 5\pi/12]$). Since the lifetime of NO_x is longer in the winter, a NO_2 maximum is expected in the winter [*Beirle et al.*, 2003]. Figure 7 shows a regional distribution of the month with the largest NO_2 abundances. It can be seen that in the east and south of China a seasonal NO_2 maximum is found according to the expected winter maximum, but in the west of China a NO_2 maximum during

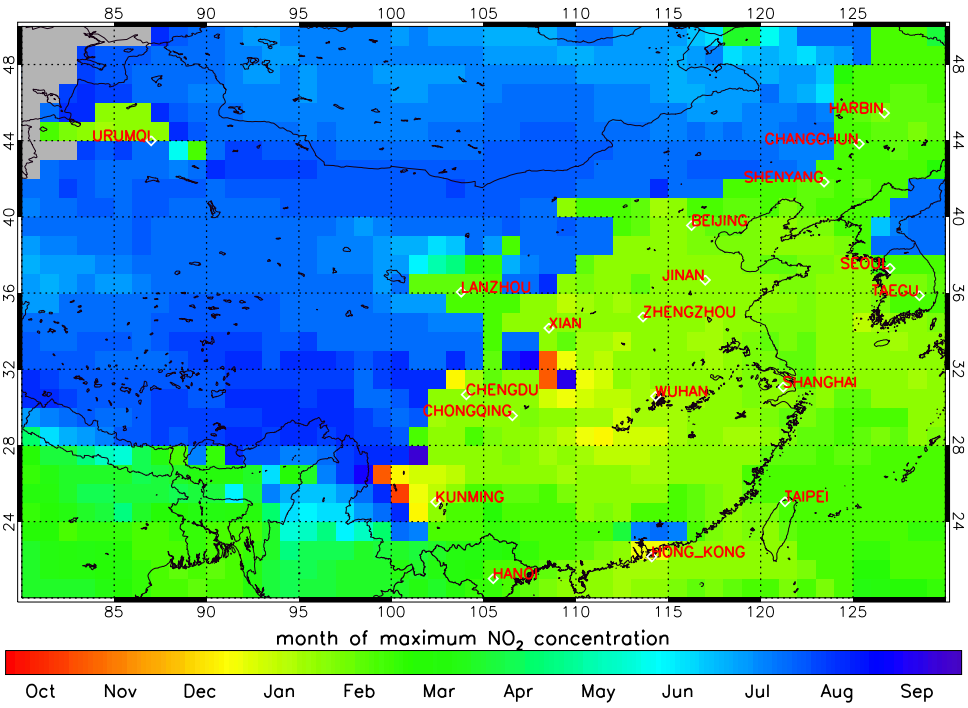

Figure 7. Map of China showing the month where the yearly seasonal component has its maximum in NO_2 concentration. In east China a maximum is found during the winter, and in the west of China a maximum is found during the summer.

summertime is found. The black grid cells correspond to regions where a linear fit works just as well but without a clear seasonal cycle. The time series in Figure 6 illustrates the winter maximum in east China. For west China the time series of the tropospheric vertical column, the stratospheric vertical column and the tropospheric air mass factor are shown in Figure 8. In Figure 8 it can be seen that the variation in the modeled air mass factor is small with respect to variations in the tropospheric NO_2 column. Figure 8 shows the expected summer maximum in the AMF and the stratospheric column as well. However, the maximum error on the tropospheric column caused by errors in the stratospheric column is 0.35 10^{15} molec/cm^2 for west China and the difference between summer and winter tropospheric columns is typical of the order 1.0 10^{15} molec/cm^2. Therefore we conclude that the air mass factor and the stratospheric NO_2 column are not the main reasons for the measured seasonal cycle of the tropospheric NO_2 column in west China.

[22] The western part of China has a low population density (see Figure 1). As a consequence natural emissions are expected to dominate the tropospheric column. Figure 7 shows that in the north west, above the large city Urumqi, a winter maximum is found, which strengthens the idea that the summer maximum in NO_2 over the rest of west China is caused by natural emissions.

[23] Lightning flash densities are measured by the Optical Transient Detector (OTD) (http://thunder.msfc.nasa.gov/otd/). From a comparison between the summer and winter flash densities can be concluded that lightning above China especially occurs during summertime when the flash rate is about 5–6 times higher than in wintertime [*Christian et al.*, 2003]. The contribution of lightning to the tropospheric NO_2 column is strongest in the tropics, with an estimated maximum of 0.4 10^{15} molec/cm^2 [*Edwards et al.*, 2003; *Boersma et al.*, 2005]. Because the difference between summer and winter tropospheric columns is typical of the order 1.0 10^{15} molec/cm^2, lightning alone cannot account for all the natural emissions in west China. *Duncan et al.* [2003] show that there is no biomass burning in the western part of China. In the work by *Yienger and Levy* [1995] it is suggested that in remote and agricultural regions soil emissions contribute 50% to the total NO_x budget and that in July these percentages can rise to more than 75%. *Yienger and Levy* [1995] also suggested that soil NO_x emissions are temperature-dependent, soil-dependent and precipitation-dependent. A higher surface temperature leads to more NO_x emissions, which would explain higher NO_x concentrations in summer time. They also found higher NO_x emissions for grassland that together with desert and scrub landform the main soil composition in west China. Another effect that increases soil NO_x emissions in summertime is "pulsing," which is described by *Yienger and Levy* [1995] and *Jaeglé et al.* [2004] as an increase in NO_x measured after a shower of rain. From the IRI/LDEO Climate Data library it can be seen that in the west part of China it is only raining in the summer season. This also contributes to enhanced NO_2 concentrations during summertime.

6. Conclusions

[24] The tropospheric NO_2 columns measured by GOME and SCIAMACHY have been used for trend analysis over China. A linear model with a seasonal component is used to fit the time series of NO_2 concentrations. By applying this

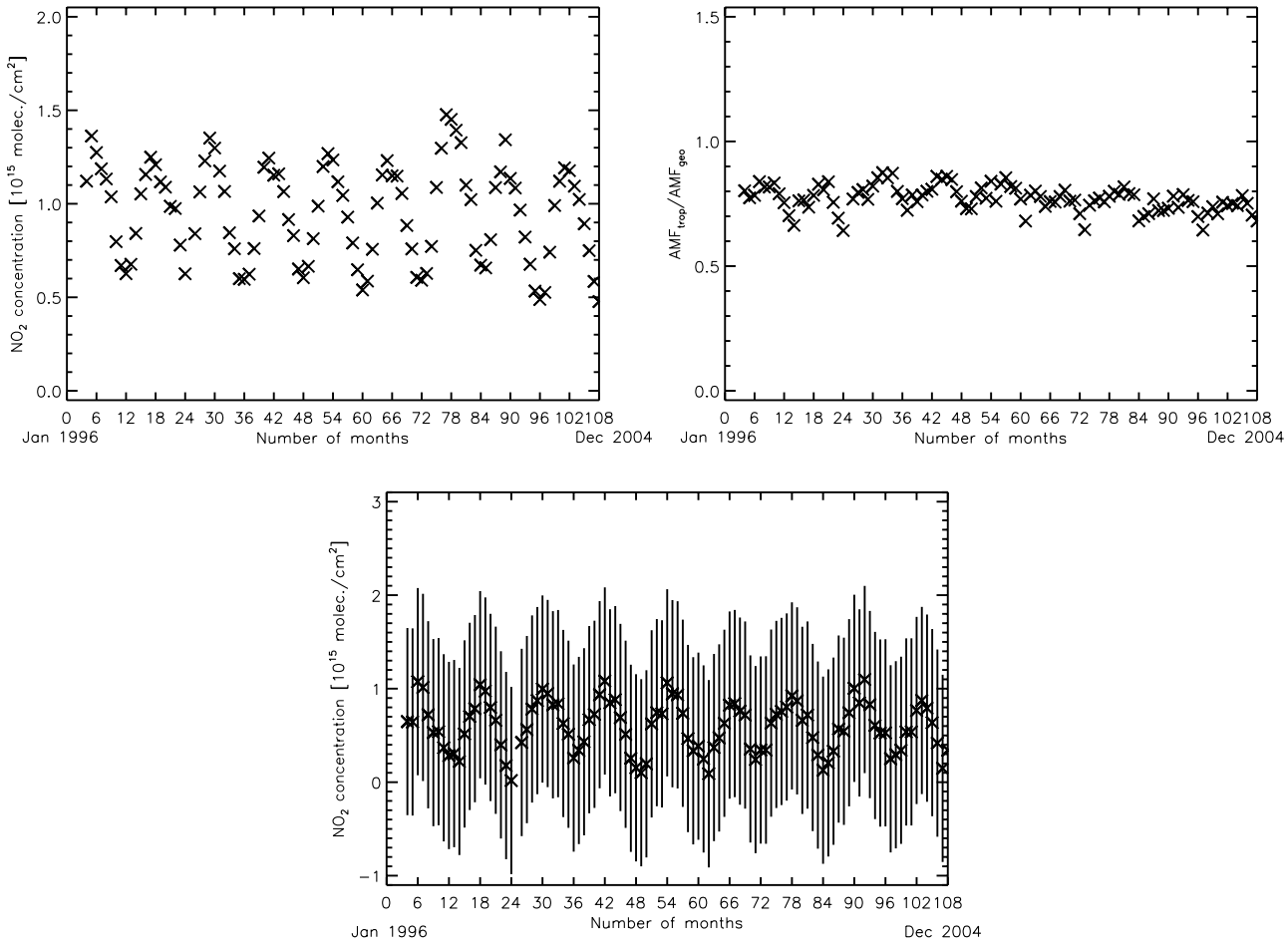

Figure 8. Time series of monthly averages of (bottom) the tropospheric vertical column, (top left) the stratospheric vertical column and (top right) the tropospheric air mass factor divided by the geometrical air mass factor. The monthly averages are calculated for west China (80–100°E, 30–42° N).

model to each grid cell a spatial distribution of the fit parameters is calculated. Furthermore the precision of the trend is calculated. It can be concluded that the 9 years long NO_2 data set from GOME and SCIAMACHY can be used for trend analysis in the eastern part of China. In this high populated and industrial area the trend is large enough to be significant. For instance Shanghai had a yearly increase of 20% ± 6% in 1996. The geographic distribution of the seasonal cycle of tropospheric NO_2 was studied. In the eastern part of China an expected winter maximum is found. In the western part of China this cycle shows a NO_2 maximum in summer time. As there is nearly no anthropogenic activity in western China, this cycle is attributed to natural emissions, especially soil emissions and lightning.

[25] The bias between the monthly GOME and SCIAMACHY tropospheric NO_2 series appears to be negligible and does not show any latitude dependence. This shows the consistency in the retrieval method of tropospheric NO_2 and allows the use of long time series by combining different instruments to detect a significant trend for regions without a large trend.

[26] It is well known that emissions are increasing over China [*Streets et al.*, 2003; *Wang and McElroy*, 2004]; this study shows that the satellite measurements are able to measure the increase of atmospheric concentrations. New emissions inventories in combination with model studies are needed to decide whether the increase in the NO_2 column is fully caused by the increase of NO_x emissions or by changes in chemical regime.

References

Beirle, S., U. Platt, M. Wenig, and T. Wagner (2003), Weekly cycle of NO_2 by GOME measurements: A signature of anthropogenic sources, *Atmos Chem. Phys.*, *3*, 2225–2232.

Boersma, K. F., H. J. Eskes, and E. J. Brinksma (2004), Error analysis for tropospheric NO_2 retrieval from space, *J. Geophys. Res.*, *109*, D04311, doi:10.1029/2003JD003962.

Boersma, K. F., H. J. Eskes, E. W. Meijer, and H. M. Kelder (2005), Estimates of lightning NO_x production from GOME satellite observations, *Atmos. Chem. Phys. Disc.*, *5*, 3047–3104.

Christian, H. J., et al. (2003), Global frequency and distribution of lightning as observed from space by the Optical Transient Detector, *J. Geophys. Res.*, *108*(D1), 4005, doi:10.1029/2002JD002347.

Dentener, F., M. van Weele, M. Krol, S. Houweling, and P. van Velthoven (2003), Trends and inter-annual variability of methane emissions derived from 1979–1993 global ctm simulations, *Atmos. Chem. Phys.*, *3*, 73–88.

Dubovik, O., et al. (2002), Climatology of aerosol absorption and optical properties in key worldwide locations, *J. Atmos. Sci.*, *59*, 590–608.

Duncan, B. N., R. V. Martin, A. C. Staaudt, R. Yevich, and J. A. Logan (2003), Interannual and seasonal variability of biomass burning emissions constrained by satellite observations, *J. Geophys. Res.*, *108*(D2), 4100, doi:10.1029/2002JD002378.

Edwards, D. P., et al. (2003), Tropospheric ozone over the tropical Atlantic: A satellite perspective, *J. Geophys. Res.*, *108*(D8), 4237, doi:10.1029/2002JD002927.

Eskes, H., and F. Boersma (2003), Averaging kernels for DOAS total-column satellite retrievals, *Atmos. Chem. Phys.*, *3*, 1285–1291.

Herman, J. R., and E. A. Celarier (1997), Earth surface reflectivity climatology at 340–380 nm from TOMS data, *J. Geophys. Res.*, *102*(D23), 28,003–28,012.

Jacob, D. J. (1999), *Introduction to Atmospheric Chemistry*, Princeton Univ. Press, Princeton, N. J.

Jaeglé, L., R. V. Martin, K. Chance, L. Steinberger, T. P. Kurosu, D. J. Jacob, A. I. Modi, V. Yoboué, L. Sigha-Nkamdjou, and C. Galy-Lacaux (2004), Satellite mapping of rain-induced nitric oxide emissions from soils, *J. Geophys. Res.*, *109*, D21310, doi:10.1029/2004JD004787.

Koelemeijer, R. B. A., J. F. de Haan, and P. Stammes (2003), A database of spectral surface reflectivity in the range 335–772 nm derived from 5.5 years of GOME observations, *J. Geophys. Res.*, *108*(D2), 4070, doi:10.1029/2002JD002429.

Leue, C., M. Wenig, T. Wagner, O. Klimm, U. Platt, and B. Jähne (2001), Quantitative analysis of NO_x emissions from Global Ozone Monitoring Experiment satellite image sequences, *J. Geophys. Res.*, *106*, 5493–5505.

Martin, R. V., et al. (2002), An improved retrieval of tropospheric nitrogen dioxide from GOME, *J. Geophys. Res.*, *107*(D20), 4437, doi:10.1029/2001JD001027.

Martin, R. V., D. J. Jacob, K. V. Chance, T. P. Kurosu, P. I. Palmer, and M. J. Evans (2003), Global inventory of nitrogen dioxide emissions constrained by space-based observations of NO_2 columns, *J. Geophys. Res.*, *108*(D17), 4537, doi:10.1029/2003JD003453.

Platt, U. (1994), Differential Optical Absorption Spectroscopy (DOAS), in *Air Monitoring by Spectroscopic Techniques*, *Chem. Anal.*, vol. 127, edited by M. W. Sigrist, pp. 27–76, Wiley-Interscience, Hoboken, N. J.

Richter, A. K., and J. P. Burrows (2002), Tropospheric NO_2 from GOME measurements, *Adv. Space Res.*, *28*, 1673–1683.

Richter, A. K., J. P. Burrows, H. Nüß, C. Granier, and U. Niemeier (2005), Increase in tropospheric nitrogen dioxide over China observed from space, *Nature*, *437*, 129–132, doi:10.1038/nature04092.

Streets, D. G., et al. (2003), An inventory of gaseous and primary aerosol emissions in Asia in the year 2000, *J. Geophys. Res.*, *108*(D21), 8809, doi:10.1029/2002JD003093.

Tiao, G., C. Reinsel, X. U. Daming, J. H. Pedrick, X. Zhu, A. J. Miller, J. J. DeLuisu, C. L. Mateer, and D. J. Wuebbles (1990), Effects of autocorrelation and temporal sampling schemes on estimates of trend and spatial correlation, *J. Geophys. Res.*, *95*, 20,507–20,517.

Vandaele, A. C., et al. (2005), An intercomparison campaign of ground-based UV-Visible measurements of NO_2, BrO, and OClO slant columns: 1. Methods of analysis and results for NO_2, *J. Geophys. Res.*, *110*, D08305, doi:10.1029/2004JD005423.

Wang, Y. X., and M. B. McElroy (2004), Asian emissions of CO and NO_x: Constraints from aircraft and Chinese station data, *J. Geophys. Res.*, *109*, D24304, doi:10.1029/2004JD005250.

Weatherhead, E. C., et al. (1998), Factors affecting the detection of trends: Statistical considerations and applications to environmental data, *J. Geophys. Res.*, *103*, 17,149–17,161.

Yienger, , J. J., Levy, and H. II (1995), Empirical model of global soil-biogenic NO_x emissions, *J. Geophys. Res.*, *100*, 11,447–11,464.

K. F. Boersma, H. Eskes, H. M. Kelder, D. H. M. U. Peters, and R. J. van der A, Royal Netherlands Meteorological Institute, NL-3730 AE De Bilt, Netherlands. (avander@knmi.nl)

I. De Smedt and M. Van Roozendael, Belgian Institute for Space Aeronomy, B-1180 Brussels, Belgium.